Journal of Power Sources 271 (2014) 278–284

Contents lists available at ScienceDirect

Journal of Power Sources

journal homepage: www.elsevier.com/locate/jpowsour

Development of rolling tin gas diffusion electrode for carbon dioxide electrochemical reduction to produce formate in aqueous electrolyte

Qinian Wang, Heng Dong*, Hongbing Yu*

Research Center for Cleaner Production, College of Environmental Science and Engineering, Nankai University, No. 94 Weijin Road, Nankai District, Tianjin 300071, China

HIGHLIGHTS

- A rolling gas diffusion electrode is developed for CO_2 electrochemical reduction.
- CO_2 electrochemical reduction is dominated by the electron transfer rate.
- Excellent Faraday efficiency towards formate formation is obtained.
- Formate is released into the electrolyte easily and the catalyst is stable.

ARTICLE INFO

Article history:
Received 15 May 2014
Received in revised form
1 August 2014
Accepted 3 August 2014
Available online 11 August 2014

Keywords:
Carbon dioxide
Electrochemical reduction
Tin
Gas diffusion electrode
Formate

ABSTRACT

Carbon dioxide electrochemical reduction to produce formate (CERPF) basing on gas diffusion electrode (GDE) is a promising carbon cycle technology. However, its performance is still restrained by formate accumulation and catalyst loss in the catalyst layer (CL). In this study, a novel rolling Sn-loading GDE (SGDE) without porous hydrophilic CL is developed. The electrochemical behavior of CERPF on the SGDE is investigated by cyclic voltammetry (CV) and electrochemical impedance spectroscopy (EIS). The electrochemical performance of the SGDE for CERPF is assessed by constant potential electrolysis. The results show that the CERPF process basing on the SGDE performs a double charge transfer and is dominated by the electron transfer rate. The highest partial current density for CERPF (17.43 ± 2.60 mA cm^{-2}) and corresponding Faraday efficiency ($78.60 \pm 0.11\%$) are obtained under the applied potential of -1.8 V vs Ag/AgCl in 0.5 M $KHCO_3$ solution. The produced formate is allowed to be released into the electrolyte easily and the catalyst holds steady during the CERPF process. Since its excellent electrochemical performance and low fabrication cost (ca. 30 \$ m^{-2}), bright prospect for SGDE application in CERPF can be convinced.

1. Introduction

Carbon dioxide (CO_2) concentration in the atmosphere now increases each year by about 2 ppm, continuing the inexorable rise toward 400 ppm and beyond [1,2]. It definitely leads to an ascent of the temperatures at the troposphere (particularly on the earth's surface), an increase in the precipitation, and a raise of the sea level [3]. Reducing CO_2 atmospheric concentration has therefore become a critical issue [4]. Many attempts have been made, such as carbon capture and sequestration [5], chemical usage [6], photochemical reduction [7], and electrochemical reduction [8]. Of those methods, electrochemical reduction can not only reduce CO_2 emission, but also produce a variety of valuable materials such as formic acid/formate, carbon monoxide, methane, ethylene, methanol, and ethanol [9] under mild conditions involving moderate temperature and atmospheric pressure [8]. Formic acid is an additive widely used in the field of medicine, chemical industries, as well as the leather industry [8]. For CO_2 electrochemical reduction to produce formate (CERPF) with aqueous electrolyte, solid electrodes are widely used while CO_2 is provided by the continuous sparging in the electrolyte. Owing to the relatively low solubility of CO_2 in water under ambient conditions (ca. 0.033 M), the current density is severely limited by the mass transfer of CO_2 from the bulk to the electrode surface. It is estimated that the mass transfer limiting current density for CERPF is 6 mA cm^{-2} [10]. In order to break through the mass transfer limitation and increase the current density for CERPF, gas diffusion electrode (GDE) has been

* Corresponding authors. Tel./fax: +86 22 23502756.
E-mail addresses: dongheng@nankai.edu.cn (H. Dong), hongbingyu1130@sina.com (H. Yu).

http://dx.doi.org/10.1016/j.jpowsour.2014.08.017
0378-7753/

introduced [4,11]. The typical GDE is a porous composite electrode, usually assembled by a gas diffusion layer (GDL), a current collector and a catalyst layer (CL) [11]. CERPF occurs in the gas–liquid–solid three phase interface (TPI), being located in the CL [11]. In the CERPF system where GDE is used as the cathode, CO_2 in the atmosphere typically diffuses through the hydrophobic region of the GDL to the reaction site (i.e. TPI) in the porous hydrophilic region of the CL [12,13]. To date, two types of GDEs have been widely used for CERPF. In the first one, the CL is composed of catalyst, carbon black and polytetrafluoroethylene (PTFE) binder, where PTFE allows forming the TPI. While the GDL consists of carbon black and PTFE binder [14]. In the second one, the CL consists of catalyst and Nafion binder, where Nafion allows forming the hydrophilic TPI. The GDL is typically made of carbon paper which is wet-proofed with PTFE [15,16]. It has been reported that the current density for CERPF can be increased by one to two orders of magnitude with GDE [10,11,14].

Although these results are exciting, several problems still need to be solved. For example, the two types of GDEs noted above are all suffering from the accumulation of liquid-phase reaction products in the reaction sites of the CL due to its porosity and hydrophilicity [10,16]. Moreover, the second GDE noted above is also suffering from catalyst loss in the CL possibly because of poor adhesion of Nafion binder [17,18]. Thus, it is necessary to develop a new GDE to solve these problems as well as achieve excellent electrochemical performance for CERPF. In addition, it is also necessary to investigate the electrochemical behavior of CERPF basing on GDE, which can give us abundant information to improve the CERPF process and electrode performance [19]. So far, the electrochemical behavior of CERPF basing on GDE is less studied [15,20–24].

In the present work, a novel rolling Sn-loading GDE (SGDE) was developed. In order to avoid the accumulation of liquid-phase reaction products, the porous hydrophilic CL is abandoned. It only consists of a GDL and a copper mesh plated with Sn, where Sn plays a role of catalysis for CERPF and the copper mesh acts as the current collector. The morphology of the SGDE was examined by scanning electron microscope (SEM). The electrochemical behavior of CERPF on the SGDE was investigated by cyclic voltammetry (CV) and electrochemical impedance spectroscopy (EIS). The assessment for the electrochemical performance of the SGDE for CERPF was carried out under constant potential electrolysis. The optimal current density and Faraday efficiency for formate production via the CERPF process on the SGDE were achieved by regulating the electrolysis potential and electrolyte concentration. In addition, the morphology and crystal structure of Sn catalyst in the SGDE before and after the constant potential electrolysis were examined by SEM and X-ray diffraction (XRD), respectively.

2. Experimental

2.1. SGDE fabrication

The SGDE consisted of a GDL and a Sn-loading copper mesh. The GDL was prepared firstly by distributing conductive carbon black (Jinqiushi Chemical Co. Ltd., Tianjin, China) into an appropriate amount of ethanol in a beaker and ultrasonic agitated for 20 min. It was followed by dripping PTFE suspensions (60 wt%, Hesen, Shanghai, China) into a blend slowly still with ultrasonic agitation. The mass ratio of conductive carbon black and PTFE was 3:7. After another 20 min, the blend was stirred at 353 K bath to give a dough-like paste. The paste was then rolled to a gas diffusion film of 0.15 mm thickness by a rolling-press device which demarcates the space of the two rolls by two pressure gages. The Sn-loading copper mesh was made as follows: the copper mesh (60 mesh, 70 μm wire diameter) was first immersed in acetone for 24 h and then etched in hydrochloric acid (10%). After washed by the distilled water, it was immersed in an electroless acidic tin plating bath consisting of 0.02 M stannous sulfate, 0.22 M sulfuric acid and 0.6 M thiourea at 319 K. Finally, the Sn-loading copper mesh was rolled on the GDL and sintered for 20 min at 613 K to obtain the final electrode of 0.2 mm thickness. More details of the SGDE (fabrication method and morphology) were described in the Supporting information (Figs. S1 and S2).

2.2. Electrochemical measurements

The electrochemical measurements containing CV and EIS were tested by an electrochemical workstation (CHI600D, Shanghai Chenhua Instruments Co., China) at ~298 K in a conventional three-compartment electrochemical cell (Fig. S3). The anodic chamber and the cathodic chamber were separated by a proton exchange membrane (PEM, Nafion117, 4 cm diameter, Dupont, USA). Specially, a gas chamber was designed. The SGDE (7 cm^2) and Pt sheet (1 cm^2, Tianjin Aidahengsheng Technology Co. Ltd., China) were chosen as the working electrode and counter electrode, respectively. The reference electrode was Ag/AgCl electrode (sat. KCl, Tianjin Aidahengsheng Technology Co. Ltd., China), being extended to the surface of the working electrode by using a Luggin capillary. All of the potential values were in reference to Ag/AgCl unless otherwise noted. The electrolyte was 0.1 M $KHCO_3$ solution. CV was conducted from −1.8 V to 0 V under different scan rates from 0.1 V s^{-1} to 1.2 V s^{-1}. EIS was performed over a frequency range of 100 kHz–0.1 Hz with the AC signal amplitude of 0.005 V superimposed on different dc potentials in the range from −1.1 V to −1.3 V. Before each measurement, the electrolyte was degassed with N_2 (99.99%, Tianjin Sizhi gas Co. Ltd., China) for 30 min for a baseline. After that N_2 or CO_2 (99.99%, Tianjin Sizhi gas Co. Ltd., China) was continuously sparged in the gas chamber through the measurement.

2.3. CERPF tests

CERPF tests were done at ~298 K under a constant potential mode in the same three-compartment electrochemical cell as described in Fig. S3, where the electrochemical reactions at both anode and cathode sides are also presented. Electrolyte was circulated by using a peristaltic pump (BT-yz1515, Tianjin Sabo Instruments Co., China) with a flow rate of 25 mL min^{-1}. The flow rate of CO_2 was 30 mL min^{-1}. An electrolytic time of 30 min was applied for each batch. The catholyte was sampled after each batch of electrolysis for analysis.

2.4. Analysis and calculation

The morphology of the SGDE was observed by using SEM (S-3500N, Hitachi Limited, Japan and SUPRA 55/55VP, ZEISS Co., Germany). The crystal structure of Sn catalyst in the SGDE was characterized by XRD (Rigaku D/MAX-2500, Cu Kα, Japan) with a scan rate of 4° min^{-1} in a 2θ range from 20° to 90°.

The Nyquist plot of impedance was simulated by Zsimpwin software (ver. 3.10).

The production of formate was analyzed by a high performance liquid chromatography (L6-P6, Beijing Puxitongyong Instruments Co., China) equipped with a C18 reversed phase column (250 mm × 4.6 mm × 5 μm) with UV detection at 210 nm. The mobile phase was 10% methanol aqueous solution at 0.6 mL min^{-1}. The pH of the liquid sample was adjusted to pH = 2 in advance. The Faraday efficiency of formate (FE) was calculated according to Equation (1) as follows:

$$FE = \frac{n_{formate} \times n \times F}{\int_0^t I dt} \times 100\% \quad (1)$$

where $n_{formate}$ is the moles of formate harvested; n represents the number of electrons required for the formation of one molecule of formate from CO_2 ($n = 2$ here); F is Faraday's constant (96,485 C mol^{-1} of electrons); and I is the circuit current.

The total current density (j_{total}) was expressed as the total current divided by the geometric area of the SGDE, while the partial current density of formate ($j_{partial}$) was expressed as the current used for forming formate divided by the geometric area of the SGDE.

3. Results

3.1. Electrochemical measurements

CV measurements were conducted to explore the electrochemical behavior of CERPF on the SGDE in 0.1 M $KHCO_3$ solution with N_2 atmosphere and CO_2 atmosphere, respectively (Fig. 1a). In N_2 atmosphere, the oxidation peak appeared at ca. −1.1 V (peak 1) while the reduction peak appeared at ca. −1.3 V (peak 2). This could be attributed to the formation and reduction of tin oxides [25] in the test solution. When scanning to the negative end of the voltammograms, an increase of the current can be observed, which should be caused by H_2 evolution reaction on the surface of the Sn-loading copper mesh side facing the electrolyte in the SGDE ($2H_2O + 2e \rightarrow H_2 + 2OH^-$) [26]. While in CO_2 atmosphere, both of the peak 1 and peak 2 shifted in the positive direction slightly and the peak current decreased (peak 1 → peak 1′ and peak 2 → peak 2′). It is noting that the reduction peak (peak 2′) became broad and less obvious and the reduction current began to go up at a potential of ca. −1.1 V. This could be attributed to the reaction between Sn catalyst and CO_2 molecule which changes the electronic density of the redox couples [27]. Thus, the increased reduction current should be caused by CERPF on the surface of the Sn-loading copper mesh side facing the electrolyte in the SGDE ($CO_2 + H_2O + 2e \rightarrow HCOO^- + OH^-$). Peak 2′ can be seen as a CERPF peak. The onset potential of CERPF was ca. −1.1 V and the peak potential (E_p) was −1.3 V, which is somewhat more positive than the value published previously on Sn solid electrode (−1.6 V vs SCE) [20]. Thanks to the SGDE, the overpotential of CERPF is decreased.

CV measurements at various scan rates were obtained on the SGDE in 0.1 M $KHCO_3$ solution with CO_2 atmosphere (Fig. 1b). The reduction peaks were all unsymmetrical and E_p clearly shifted toward more negative potential with an increase of the scan rate, indicating that the CERPF process was irreversible [28–30]. This agrees with the results reported on the solid electrodes [20,21,31]. The reduction peak current (I_p) was proportional to the scan rate (v) over the range from 0.1 V s^{-1} to 0.5 V s^{-1} (Fig. 1b, insert plot, $R^2 > 0.99$), suggesting that the CERPF process was dominated by the electron transfer rate (i.e. CERPF was a surface-tethered redox functionality process) [28,32]. Nevertheless, when the scan rate was greater than 0.5 V s^{-1}, I_p was proportional to neither v nor $v^{0.5}$. This possibly indicates that the CERPF process is dominated by the mass transfer rate and the electron transfer rate simultaneously. This is different from the results reported on the solid electrodes, where the CERPF process was just dominated by the mass transfer rate (i.e. CERPF was a mass transfer limited process) [31,33]. This is to say, the SGDE can effectively conquer the mass transfer limitation.

For an irreversible electrode reaction, the relationship between peak potential (E_p) and scan rate (v) follows Laviron's equation [34].

$$E_p = E^{o\prime} - \frac{RT}{n\alpha F}\ln\left(\frac{n\alpha F v}{RTk_s}\right) \quad (2)$$

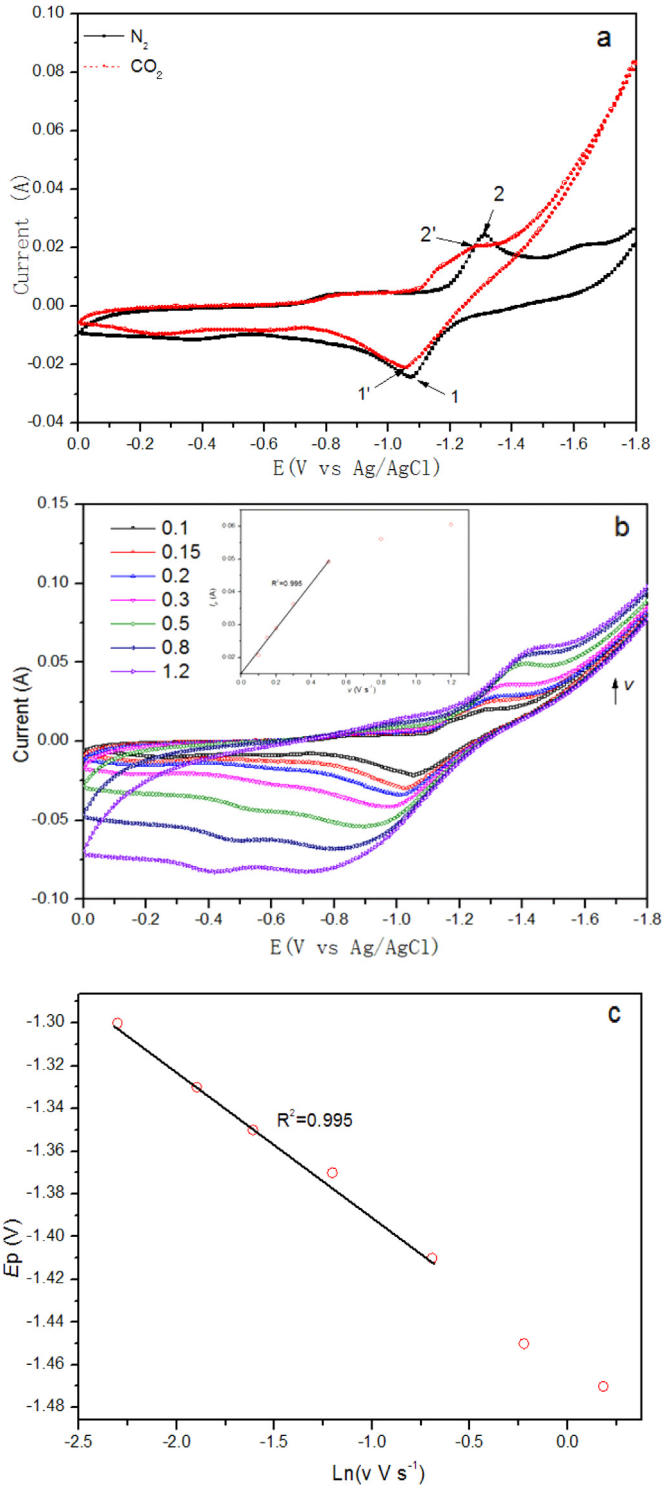

Fig. 1. (a) CV of CERPF on the SGDE in 0.1 M $KHCO_3$ solution with N_2 atmosphere and CO_2 atmosphere at the scan rate of 0.1 V s^{-1}; (b) a series of CVs on the SGDE at the scan rate from 0.1 V s^{-1} to 1.2 V s^{-1}, the inserted plot is the variation of the reduction peak current with the scan rate; (c) variation of the reduction peak potential with the natural logarithm of the scan rate.

Where $E^{o\prime}$ is the formal potential (V), R is the universal gas constant (8.314 J mol^{-1} K^{-1}), T is the absolute temperature (K), n is the number of electrons transferred, α is the electron transfer coefficient, F is the Faraday constant (96,485 C mol^{-1}), k_s is the standard rate constant (s^{-1}), v is the scan rate (V s^{-1}).

Fig. 1c shows the plot of E_p vs ln v. $E^{o\prime}$ can be obtained from the intercept of plot E_p vs v [35]. When v lower than 0.5 V s^{-1}, the plot of E_p vs v was a linear ($R^2 > 0.99$). The equation of the straight line was

$$E_p = -0.066 \ln v - 1.454 \quad (3)$$

According to Equations (2) and (3), $n\alpha$ was evaluated to be 0.39 and k_s to be 1.23 s^{-1}. Referring to the results published previously [20,21,31,36], it is estimated that the CERPF process is a single electron transfer reaction ($n = 1$). So α was evaluated to be 0.39, which is close to the values published on the solid electrodes previously [37].

Tafel plot was used to assess the kinetic performance of CERPF on the SGDE in 0.1 M $KHCO_3$ solution with CO_2 atmosphere. It was obtained according to the voltammograms (Fig. 1a) and is shown in Fig. 2. The linear region of the plot obeys the Tafel equation [28], which relates the overpotential (η) to the current density (j). Parameters obtained from the plot are presented in Table 1. A revealing feature of the Tafel plot was the occurrence of two Tafel regions. One was at lower overpotential with a slope of 174 mV $decade^{-1}$ (region 1) and the other one was at higher overpotential with a slope of 542 mV $decade^{-1}$(region 2). A Tafel slope of 185 mV $decade^{-1}$ at lower overpotential and 458 mV $decade^{-1}$ at higher overpotential on Sn GDE in 0.5 M $NaHCO_3$ solution were reported by Prakash et al. [15]. The value obtained at lower overpotential region in this study agrees fairly well with the reported one. While the value obtained at higher overpotential is somewhat higher but still on the same order as the reported one. The equilibrium potential (E_{eq}) obtained on the SGDE (−0.4 V) is close to the results reported on the Sn solid electrodes under similar conditions (−0.11 V vs NHE) [15,38]. The exchange current density j_0 obtained on the SGDE at lower overpotential (7.78×10^{-8} A cm^{-2}) is different by three to four orders of magnitude from the one reported by Prakash et al. on Sn GDE in 0.5 M $NaHCO_3$ solution (1.60×10^{-4} A cm^{-2}) [15]. Such a difference may be caused by the electrolyte concentration and cation used for the measurement [39].

The electrochemical behavior of CERPF on the SGDE was further surveyed by EIS measurements with CO_2 atmosphere. Since the onset potential of CERPF was ca. −1.1 V (see CV results), the applied potential was set at −1.1 V, −1.2 V and −1.3 V in turn, where the corresponding overpotential was 0.7 V, 0.8 V and 0.9 V, respectively. When the overpotential was 0.7 V, the Nyquist plot showed one semicircle (Fig. 3a) and could be modeled by equivalent circuit

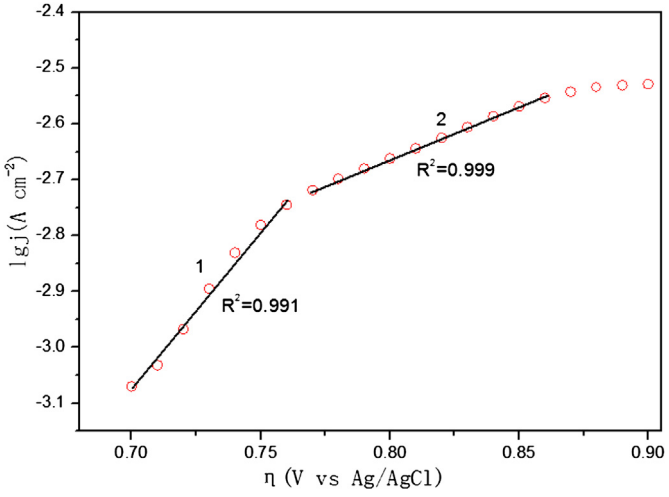

Fig. 2. Tafel plot obtained from the corresponding voltammograms.

Table 1
Tafel parameters obtained from the corresponding Tafel plot.

	Region 1	Region 2
Fitting equation	$y = 5.762x - 7.109$	$y = 1.846x - 4.139$
b (mV $decade^{-1}$)	174	542
j_0 (A cm^{-2})	7.78×10^{-8}	7.26×10^{-5}

model (ECM) i (Fig. 3b). When the overpotential was 0.8 V and 0.9 V, the plots presented two semicircles with two different time constants (Fig. 3a) and could be modeled by ECM ii (Fig. 3b). The parameters obtained from the EIS fitting procedure are given in Table 2 (fitting errors < 10%).

The solution resistances (R_s) were all similar at different overpotential due to the same cell, fixed reference electrode and electrolyte were used in the EIS measurements. Under the same overpotential (0.8 V and 0.9 V), the charge transfer resistances (R_2) were all higher than the ohm resistances (R_1) and the solution resistances (R_s), indicating that the electron transfer rate dominated the CERPF process. It is in accord with the CV results. Moreover, R_1 and R_2 decreased with an increase of the overpotential from 0.8 V to 0.9 V. The minimum R_1 (1.85 Ω) and R_2 (8.34 Ω) were both obtained at the overpotential of 0.9 V, which were approximately 8.41% and 40.00% lower than that obtained at the overpotential of 0.8 V (R_1: 2.02 Ω, R_2: 13.90 Ω), respectively. This is to say, the increase of the overpotential can accelerate the CERPF process. In fact, the changes of R_1 at different overpotential are insignificant when taking the fitting errors into consideration (<10%). Thus, the main reason for accelerating the CERPF process can be attributed to the decrease of R_2.

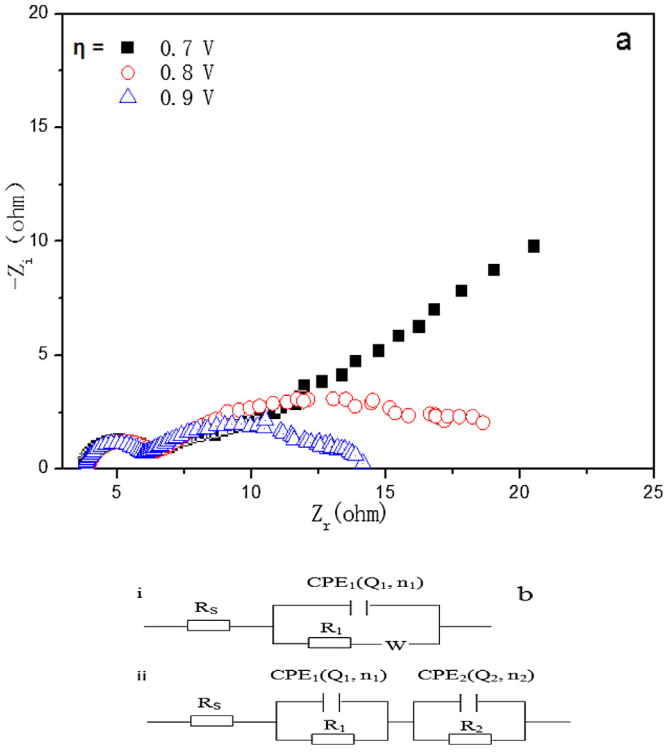

Fig. 3. (a) Nyquist plots of impedance measured at different overpotential on the SGDE with 0.1 M $KHCO_3$ solution and CO_2 atmosphere; (b) equivalent circuit used for the fitting of the impedance plots (i) 1-CPE model, (ii) 2-CPE model; R_s: solution resistance, R_1: ohm resistance, W: Warburg impedance, R_2: charge transfer resistance, CPE_1 and CPE_2: constant phase angle element, Q_1: CPE_1 value, Q_2: CPE_2 value, n_1: coefficient of CPE_1, n_2: coefficient of CPE_2.

Table 2
Simulated data of equivalent circuits for the Nyquist plots of impedance.

η (V)	R_S (Ω)	Q_1 (F)	n_1	R_1 (Ω)	Q_2 (F)	n_2	R_2 (Ω)	W (Ω)
0.7	3.56	1.40×10^{-4}	0.74	3.67	–	–	–	2.84×10^{-2}
0.8	3.91	1.01×10^{-5}	1	2.02	7.97×10^{-3}	0.56	13.90	–
0.9	3.77	9.29×10^{-6}	1	1.85	8.13×10^{-3}	0.57	8.34	–

The Warburg impedance (W) was obviously observed at the overpotential of 0.7 V, but the value (2.84×10^{-2} Ω) was much lower than other resistances (R_s, R_1 and R_2). As the overpotential was increased (0.8 V and 0.9 V), W became inconspicuous. In addition, W appears only when R_2 is not the dominant resistance [40]. It is confirmed that the CERPF process on the SGDE is not dominated by the mass transfer rate, having been obtained from the CV results.

Q_1 and Q_2 are capacitances, corresponding to R_1 and R_2. They are distributed according to the difference in the magnitude of the time constants between ohm and kinetic processes. As shown in Table 2, Q_2 was approximately 7.97×10^2 and 1.02×10^3 times higher than Q_1 at the overpotential of 0.8 V and 0.9 V, respectively. It can be ascribed to the high surface area when charge transfer occurs [41]. Moreover, Q_1 and Q_2 did not change significantly with an increase in the overpotential from 0.8 V to 0.9 V. These results are in conformity with the previous conclusion that the capacitance is related to the surface area or porosity of an electrode [42,43].

3.2. CERPF tests

The influences of the $KHCO_3$ concentration and electrolysis potential on the CERPF were discussed.

3.2.1. Influence of $KHCO_3$ concentration

In order to determine the influence of the $KHCO_3$ concentration on the CERPF, a series of electrolysis experiments under the applied potential of −1.8 V were carried out in $KHCO_3$ solutions with different concentrations (0.1, 0.3, 0.5, 0.7, 0.9 M). As shown in Fig. 4, the partial current density of formate ($j_{partial}$) increased as the $KHCO_3$ concentration increased from 0.1 M to 0.5 M. When the $KHCO_3$ concentration increased further to 0.9 M, $j_{partial}$ began to decrease. The maximum $j_{partial}$ of 17.43 ± 2.60 mA cm^{-2} was reached when the $KHCO_3$ concentration was 0.5 M, which was approximately 7.14 and 1.40 times higher than that when the $KHCO_3$ concentration was 0.1 M (2.44 ± 0.05 mA cm^{-2}) and 0.9 M (12.49 ± 1.02 mA cm^{-2}), respectively.

Other than $j_{partial}$, the Faraday efficiency is also a widely used figure of merit to assess the performance of an electrochemical process. As shown in Fig. 4, the variation tendency of the Faraday efficiency of formate (FE) with the $KHCO_3$ concentration was the same as the above-mentioned. The maximum FE of 78.60 ± 0.11% was reached also when the $KHCO_3$ concentration was 0.5 M, which were approximately 2.94 and 1.75 times higher than that when the $KHCO_3$ concentration was 0.1 M (26.74 ± 1.20%) and 0.9 M (44.81 ± 3.50%), respectively. Hence the optimal $KHCO_3$ concentration for CERPF in this study was 0.5 M, which is in accord with the results published previously [9,36,44].

3.2.2. Influence of applied potential

A series of electrolysis experiments were carried out in 0.5 M $KHCO_3$ solutions with different applied potential in the range from −1.2 V to −2.2 V at 0.2 V intervals. As shown in Fig. 5, $j_{partial}$ increased when the applied potential shifted in negative direction to −1.8 V, but it decreased when the applied potential shifted from −1.8 V to −2.2 V. The maximum $j_{partial}$ (17.43 ± 2.60 mA cm^{-2}) was obtained under the applied potential of −1.8 V, which was approximately 52.82 and 1.12 times higher than that under the applied potential of −1.2 V (0.33 ± 0.05 mA cm^{-2}) and −2.2 V (15.60 ± 0.87 mA cm^{-2}), respectively. The variation tendency of FE with the applied potential was the same as the $j_{partial}$. The maximum FE of 78.60 ± 0.11% was reached under the applied potential of −1.8 V, which was approximately 3.14 and 1.79 times higher than that under the applied potential of −1.2 V (25.00 ± 2.00%) and −2.2 V (44.00 ± 1.00%), respectively. Hence the optimal applied potential for CERPF in this study was −1.8 V, which is in accord with the results published previously [15,17,26].

4. Discussion

CERPF is a complex electrochemical process, whose $j_{partial}$ and FE are highly dependent on the catalyst, local pH, electrolysis potential and electrolyte [15]. So far, there is still some controversy regarding the mechanism of CERPF, intimately associated with its electrochemical behavior [15]. It is thus required to be discussed in this work. CV has been widely employed for the electrochemical behavior of CERPF. Nevertheless, as already stated by other authors, CV alone could not offer enough information [45]. Other than CV, EIS was proved to be a useful tool to gain more insight about this reaction in this study. In EIS measurements (Fig. 3), when the overpotential was 0.8 V and 0.9 V, the impedance behavior

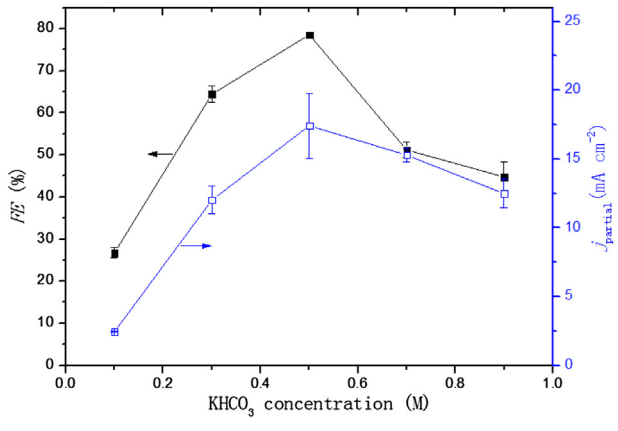

Fig. 4. Variations of partial current density and Faraday efficiency of formate on the SGDE with different $KHCO_3$ concentration.

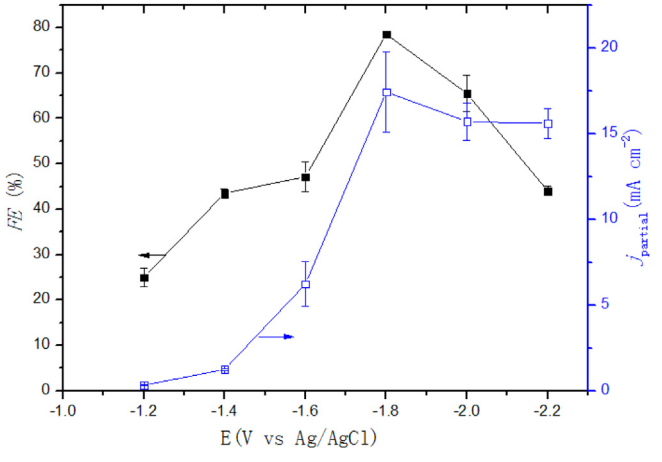

Fig. 5. Variations of partial current density and Faraday efficiency of formate on the SGDE with different applied potential.

corresponded to two successive electron transfers involving an adsorbed intermediate [24,46]. This was different from the overpotential of 0.7 V. Considering that the onset potential of CERPF was ca. −1.1 V (corresponding overpotential was ca. 0.7 V, see CV results), we may announce that CERPF occurred under the overpotential of 0.8 V and 0.9 V. In Tafel plot measurements (Fig. 2), two Tafel regions with their relative respective slopes were observed, confirming that the CERPF process performed in two consecutive steps. Moreover, this is common to the most electrodes used in aqueous electrolyte [44,47]. Considering that the only common intermediate step for the CERPF process is CO_2 (ad) + e → CO_2^- (ad) [19] that needs energy input along with the EIS results (Fig. 3), the mechanism of CERPF on the SGDE is possibly depicted as follows:

$$CO_2(g) \rightarrow CO_2(ad) \quad (4)$$

$$CO_2(ad) + e \rightarrow CO_2^-(ad) \quad (5)$$

$$CO_2^-(ad) + H_2O + e \rightarrow HCOO^-(ad) + OH^- \quad (6)$$

$$HCOO^-(ad) \rightarrow HCOO^-(aq) \quad (7)$$

The proposed mechanism could explain the existence of two different time constants and two successive Tafel regions with their relative respective slopes found in this study. The first electron transfer reaction is the formation of the radical anion CO_2^- (ad) and its existence has been proved by spectroscopic techniques [48]. The formation of CO_2^- (ad) is not easy since a large reorganizational energy between liner molecule and bent radical anion is needed. In CERPF tests, when more negative potential was applied (from −1.2 V to −1.8 V in this study), a large number of CO_2^- (ad) supply became possible. Therefore, the production of formate was increased. At the same time, the side reactions almost had not been launched. When the applied potential was more negative than −1.8 V, the side reactions (such as H_2 evolution reaction) emerged. Therefore, the production of formate began to decrease.

For the CERPF process, the $KHCO_3$ concentration is a crucial factor. Firstly, $KHCO_3$ electrolyte has buffer ability to neutralize OH^- (generated from Equation (6)). Low $KHCO_3$ concentration would lead to weak buffer ability and high pH, which restrains the CERPF process [26,36]. While high $KHCO_3$ concentration can keep the pH of electrolyte steady but low which promotes H_2 evolution reaction in the mean time. Secondly, a higher $KHCO_3$ concentration will bring better ionic conductivity which is beneficial to j_{total} [36]. It was also found in this study (data not show). Finally, the $KHCO_3$ electrolyte can produce reactant CO_2 due to the homogenous acid–base reactions [36] ($HCO_3^- \rightleftharpoons CO_2 + OH^-$, $CO_3^{2-} + 2H_2O \rightleftharpoons OH^- + HCO_3^-$). Hence the optimal $KHCO_3$ concentration for CERPF should exist and the value was 0.5 M in our conditions.

The maximum $j_{partial}$ (17.43 ± 2.60 mA cm^{-2}) for CERPF in this study and the corresponding FE (78.60 ± 0.11%) were obtained under the applied potential of −1.8 V in 0.5 M $KHCO_3$ solution (corresponding j_{total} was 22.17 ± 3.30 mA cm^{-2}). This FE is one of the highest values found in the literature using Sn electrodes under similar conditions [11,15,18,36,49–52]. For example, Köleli et al. reported a FE of 68.00% with j_{total} less than 1 mA cm^{-2} by use of Sn solid electrode [49]. While Machunda et al. obtained a FE of 18% with j_{total} of ca. 2 mA cm^{-2} by use of Sn GDE [18]. Obviously, our results (j_{total}: 22.17 ± 3.30 mA cm^{-2}, FE: 78.60 ± 0.11%) are better than all of those values (j_{total} and FE). Recently, Prakash et al. reported a FE of 70% with j_{total} of 27 mA cm^{-2} [15] on Sn GDE, which could be comparable with our results in this study.

Comparing with Sn solid electrode, the SGDE has a great advantage in breaking through the mass transfer limitation.

In theory, the SGDE changes CO_2 transfer path radically. The transfer path of CO_2 from the bulk to the electrode surface by use of Sn solid electrode is changed to that from the GDL to the electrode surface (i.e. the surface of the Sn-loading copper mesh side facing the electrolyte) by use of the SGDE. Owing to the abundant hydrophobic pores in the GDL (see Fig. S2), CO_2 can diffuse through the GDL to the electrode surface from the atmosphere more conveniently than that from the bulk. Moreover, CO_2 (ad) can directly be obtained from CO_2 (g) (CO_2 (g) → CO_2 (ad)) by use of the SGDE rather than CO_2 (aq) ($CO_2(g) \rightarrow CO_2(aq) \rightleftharpoons CO_2(ad)$) by use of Sn solid electrode. So that the SGDE can effectively increase the concentration of CO_2 (ad) on the electrode surface, which is the main reactants for CERPF. Thus, the electrochemical performance of CERPF on the SGDE is improved.

The advantage of the SGDE is also confirmed in our experiments. According to the analysis for CV and EIS measurements above, the CERPF process basing on the SGDE was dominated by the electron transfer rate. It was clearly in EIS measurement that the charge transfer resistance was higher than other resistances under the applied potential where the CERPF process occurred, indicating that the CERPF process was dominated by electron transfer rate. Moreover, the Warburg impedance disappeared when the CERPF process occurred. This further indicated that the CERPF process basing on the SGDE was not a mass transfer limited process. In CERPF tests, the electrochemical performance of CERPF basing on the SGDE (j_{total}: 22.17 ± 3.30 mA cm^{-2}, FE: 78.60 ± 0.11%) was more excellent than that basing on Sn solid electrode (e.g. j_{total}: <1 mA cm^{-2}, FE: 68.00%), where electrochemical performance was severely limited by the mass transfer.

As to the large scale production and industrial application, some properties of the SGDE including the stability of the catalyst, the fabrication cost and production desorption should be considered.

The morphology and crystal structure of Sn catalyst in the SGDE before and after the CERPF experiment under the applied potential of −1.8 V in 0.5 M $KHCO_3$ solution were examined by SEM and XRD, which are shown in the Supporting information (Figs. S4 and S5). It can be seen that the crystallite orientations, intensities and microstructure surface of Sn catalyst in the SGDE did not change significantly after the CERPF process, indicating that Sn catalyst plated on the SGDE was rather stable. In addition, the SGDE can be fabricated easily and its fabrication cost is low (ca. 30 $ m^{-2}). This is a progress compared to some of the previous works on GDE [17,18]. Moreover, with the unique structure of the SGDE (without porous hydrophilic CL), the liquid-phase reaction products (e.g. formate) can be released to the electrolyte easily (see EIS results above). It directly contributes to the excellent electrochemical performance of the SGDE by avoiding the accumulation of the liquid-phase reaction products.

5. Conclusions

A novel rolling Sn-loading (electroless tin plating) GDE (SGDE) was developed for CO_2 electrochemical reduction to produce formate (CERPF). It can break through CO_2 mass transfer limitation found in the solid electrode. The highest partial current density for CERPF (17.43 ± 2.60 mA cm^{-2}) and corresponding Faraday efficiency (78.60 ± 0.11%) were obtained under the applied potential of −1.8 V in 0.5 M $KHCO_3$ solution, which is the top one among the reported results of CERPF using Sn GDE. The Sn catalyst plated on the SGDE was rather stable during the CERPF process. The fabrication cost is low (ca. 30 $ m^{-2}). The liquid-phase reaction products (e.g. formate) can be released to the electrolyte effortlessly. These advantages of the SGDE would greatly promote the CERPF application in industry.

Acknowledgments

The authors gratefully acknowledge the Major National Science & Technology Projects of China on Water Pollution Control and Treatment (2012ZX07501002-001) for the financial support.

Appendix A. Supplementary data

Supplementary data related to this article can be found at http://dx.doi.org/10.1016/j.jpowsour.2014.08.017.

Nomenclature

GDE	gas diffusion electrode
GDL	gas diffusion layer
CL	catalyst layer
TPI	three phase interface
PTFE	polytetrafluoroethylene

References

[1] E.J. Maginn, J. Phys. Chem. Lett. 1 (2010) 3478–3479.
[2] H.Z. Zhao, Y. Zhang, Y.Y. Chang, Z.S. Li, J. Power Sources 217 (2012) 59–64.
[3] J. Lee, Y. Kwon, R.L. Machunda, H.J. Lee, Chem. Asian J. 4 (2009) 1516–1523.
[4] A. Taheri Najafabadi, Int. J. Energy Res. 37 (2013) 485–499.
[5] A. Skorek-Osikowska, J. Kotowicz, K. Janusz-Szymańska, Energy Fuels 26 (2012) 6509–6517.
[6] X. Xiaoding, J. Moulijn, Energy Fuels 10 (1996) 305–325.
[7] P. Furler, J. Scheffe, M. Gorbar, L. Moes, U. Vogt, A. Steinfeld, Energy Fuels 26 (2012) 7051–7059.
[8] M. Alvarez-Guerra, S. Quintanilla, A. Irabien, Chem. Eng. J. 207–208 (2012) 278–284.
[9] M. Jitaru, J. Univ. Chem. Technol. Metallurgy 42 (2007) 333–344.
[10] C. Oloman, H. Li, ChemSusChem 1 (2008) 385–391.
[11] M. Mahmood, D. Masheder, C. Harty, J. Appl. Electrochem. 17 (1987) 1159–1170.
[12] K.R. Lee, J.H. Lim, J.K. Lee, H.S. Chun, Korean J. Chem. Eng. 16 (1999) 829–836.
[13] H. Dong, H. Yu, X. Wang, Environ. Sci. Technol. 46 (2012) 13009–13015.
[14] C.M. Sánchez-Sánchez, V. Montiel, D.A. Tryk, A. Aldaz, A. Fujishima, Pure Appl. Chem. (2001) 1917.
[15] G.K.S. Prakash, F.A. Viva, G.A. Olah, J. Power Sources 223 (2013) 68–73.
[16] J. Wu, P.P. Sharma, B.H. Harris, X.D. Zhou, J. Power Sources 258 (2014) 189–194.
[17] S. Lee, H. Ju, H. Jeon, R.L. Machunda, D. Kim, J.K. Lee, J. Lee, ECS Trans. 53 (2013) 41–47.
[18] R.L. Machunda, H. Ju, J. Lee, Curr. Appl. Phys. 11 (2011) 986–988.
[19] R. Chaplin, A. Wragg, J. Appl. Electrochem. 33 (2003) 1107–1123.
[20] B.R. Eggins, J. McNeill, J. Electroanal. Chem. Interfacial Electrochem. 148 (1983) 17–24.
[21] B.R. Eggins, E.M. Bennett, E.A. McMullan, J. Electroanal. Chem. 408 (1996) 165–171.
[22] H. De Jesús-Cardona, C. del Moral, C.R. Cabrera, J. Electroanal. Chem. 513 (2001) 45–51.
[23] H. Zhao, Y. Chang, C. Liu, J. Porphyrins Phthalocyanines 17 (2013) 259–263.
[24] V. Lates, A. Falch, A. Jordaan, R. Peach, R.J. Kriek, Electrochim. Acta 128 (2014) 75–84.
[25] S. Kapusta, N. Hackerman, Electrochim. Acta 25 (1980) 1625–1639.
[26] W. Lv, R. Zhang, P. Gao, L. Lei, J. Power Sources 253 (2014) 276–281.
[27] M. Isaacs, F. Armijo, G. Ramírez, E. Trollund, S. Biaggio, J. Costamagna, M.J. Aguirre, J. Mol. Catal. A Chem. 229 (2005) 249–257.
[28] A.J. Bard, L.R. Faulkner, Electrochemical Methods: Fundamentals and Applications, Wiley, New York, 1980.
[29] H. Tang, Y.D. Yan, M.L. Zhang, Y. Xue, Z.J. Zhang, W.C. Du, H. He, Acta Phys. Chim. Sin. 29 (2013) 1698–1704.
[30] M.L. Zhang, L.J. Chen, W. Han, Y.D. Yan, P. Cao, Trans. Nonferrous Met. Soc. China 22 (2012) 711–716.
[31] L. Zhang, Y. Luo, D. Niu, L. Xiao, J. Lu, Chem. J. Chinese U. 28 (2007) 1660.
[32] H. Luo, Z. Shi, N. Li, Z. Gu, Q. Zhuang, Anal. Chem. 73 (2001) 915–920.
[33] B. Innocent, D. Liaigre, D. Pasquier, F. Ropital, J.M. Léger, K. Kokoh, J. Appl. Electrochem. 39 (2009) 227–232.
[34] E. Laviron, J. Electroanal. Chem. Interfacial Electrochem. 101 (1979) 19–28.
[35] M. Xiaomei, H. Jingbo, S. Jun, L. Qilong, Chin. J. Anal. Chem. 32 (2004) 1027–1030.
[36] J. Wu, F.G. Risalvato, F.S. Ke, P. Pellechia, X.D. Zhou, J. Electrochem. Soc. 159 (2012) F353–F359.
[37] W. Paik, T. Andersen, H. Eyring, Electrochim. Acta 14 (1969) 1217–1232.
[38] B.P. Sullivan, K. Krist, H. Guard, Electrochemical and Electrocatalytic Reactions of Carbon Dioxide, Access Online via Elsevier, 1992.
[39] Y.B. Vassiliev, V. Bagotsky, N. Osetrova, O. Khazova, N. Mayorova, J. Electroanal. Chem. Interfacial Electrochem. 189 (1985) 271–294.
[40] X. Li, X. Wang, Y. Zhang, N. Ding, Q. Zhou, Appl. Energy 123 (2014) 13–18.
[41] X.H. Yang, Y.Y. Xia, J. Solid State Electrochem. 14 (2010) 109–114.
[42] M. Mirzaeian, P.J. Hall, J. Power Sources 195 (2010) 6817–6824.
[43] H. Dong, H. Yu, X. Wang, Q. Zhou, J. Feng, Water Res. 46 (2012) 5777–5787.
[44] M. Jitaru, D. Lowy, M. Toma, B. Toma, L. Oniciu, J. Appl. Electrochem. 27 (1997) 875–889.
[45] M. Gattrell, N. Gupta, A. Co, J. Electroanal. Chem. 594 (2006) 1–19.
[46] E. Barsoukov, J.R. Macdonald, Impedance Spectroscopy: Theory, Experiment, and Applications, John Wiley & Sons, 2005.
[47] Y.B. Vasiliev, V. Bagotskii, N. Osetrova, J. Electroanal. Chem. 189 (1985) 271–294.
[48] H. Noda, S. Ikeda, A. Yamamoto, H. Einaga, K. Ito, Bull. Chem. Soc. Jpn. 68 (1995) 1889–1896.
[49] F. Köleli, T. Atilan, N. Palamut, A. Gizir, R. Aydin, C. Hamann, J. Appl. Electrochem. 33 (2003) 447–450.
[50] M. Azuma, K. Hashimoto, M. Hiramoto, M. Watanabe, T. Sakata, J. Electrochem. Soc. 137 (1990) 1772–1778.
[51] A.S. Agarwal, Y. Zhai, D. Hill, N. Sridhar, ChemSusChem 4 (2011) 1301–1310.
[52] H. Li, C. Oloman, J. Appl. Electrochem. 35 (2005) 955–965.